

Sub-Eddington Star-Forming Regions are Super-Eddington: Momentum Driven Outflows from Supersonic Turbulence

Todd A. Thompson¹ & Mark R. Krumholz²

¹*Department of Astronomy and Center for Cosmology & Astro-Particle Physics, The Ohio State University, Columbus, Ohio 43210*

²*Department of Astronomy and Astrophysics, University of California, Santa Cruz, CA 95064, USA*

15 July 2021

ABSTRACT

We show that the turbulent gas in the star-forming regions of galaxies is unstable to wind formation via momentum deposition by radiation pressure or other momentum sources like supernova explosions, even if the system is below the average Eddington limit. This conclusion follows from the fact that the critical momentum injection rate per unit mass for unbinding gas from a self-gravitating system is proportional to the gas surface density and that a turbulent medium presents a broad distribution of column densities to the sources. For an average Eddington ratio of $\langle \Gamma \rangle \simeq 0.1$ and for turbulent Mach numbers $\gtrsim 30$, we find that $\sim 1\%$ of the gas is ejected per dynamical timescale at velocities larger than the local escape velocity. Because of the lognormal shape of the surface density distribution, the mass loss rate is highly sensitive to the average Eddington ratio, reaching $\sim 20 - 40\%$ of the gas mass per dynamical time for $\langle \Gamma \rangle \simeq 1$. Using this model we find a large scatter in the mass-loading factor for star-forming galaxies, ranging from $\sim 10^{-3} - 10$, but with significant uncertainties. Implications for the efficiency of star formation in giant molecular clouds are highlighted. For radiation pressure feedback alone, we find an increasing star formation efficiency as a function of initial gas surface density. Uncertainties are discussed.

Key words: galaxies: formation, evolution, starburst — galaxies: star clusters: general

1 INTRODUCTION

Momentum deposition in the interstellar medium (ISM) by radiation pressure on dusty gas and/or supernovae has been discussed as a mechanism for driving turbulence and launching winds in rapidly star-forming galaxies (e.g., Harwit 1962; Scoville 2003; Murray et al. 2005; Thompson et al. 2005; Murray et al. 2011; Hopkins et al. 2012; Zhang & Thompson 2012; Ostriker & Shetty 2011; Shetty & Ostriker 2012; Faucher-Giguere et al. 2013), and in disrupting the giant molecular clouds (GMCs) around forming star clusters (e.g., O’dell et al. 1967; Scoville et al. 2001; Krumholz & Matzner 2009; Murray et al. 2010; Fall et al. 2010; Krumholz & Dekel 2010; Murray et al. 2011; Dekel & Krumholz 2013; Skinner & Ostriker 2015). Virtually all semi-analytic treatments to date calculate the dynamics by considering the interaction between a gaseous medium with a specified set of mean properties. In these models, the behavior of the system is primarily determined by $\langle \Gamma \rangle$, the average Eddington ratio that describes the balance between momentum injection and gravity.

Thompson et al. (2005) compared predictions for radiation pressure — plus supernova — supported interstellar media with observations of ultra-luminous infrared galaxies (ULIRGs) and found that the observed fluxes were close to the theoretical predictions

on $\lesssim 200 - 300$ pc scales in these extreme systems. Andrews & Thompson (2011) compared the dusty Eddington limit with data for a broad range of galaxies, including galaxy-averaged observations of normal spirals and starbursts, individual subregions of resolved galaxies in the local universe, and ULIRGs at high redshift. They showed that normal galaxies in general fall below $\langle \Gamma \rangle \sim 1$ and that the Eddington limit presents an upper bound to the fluxes observed. Andrews & Thompson (2011) also showed that inferences about whether or not galaxies as a whole reach the Eddington limit are hampered by uncertainties in the CO/HCN-H₂ conversion factors and dust-to-gas ratio (see also Faucher-Giguere et al. 2013), and by time-dependent effects in big spirals where the majority of the area is not star forming at a given time. They found that $\langle \Gamma \rangle$ generally *decreased* for higher average gas surface density galaxies and (similarly) that $\langle \Gamma \rangle$ increases as a function of galactocentric radius in galaxies, generically because the gas surface density falls. This behavior follows from the fact that the “single-scattering Eddington flux” increases more rapidly with gas surface density than does the observed bolometric flux from galaxies.¹ Recent work by Coker et al. (2013) on the wind of M82 also shows that it is sub-

¹ This is equivalent to the statement that observational determinations of the star formation rate per unit area as a function of gas surface density

Eddington on kpc scales along its minor axis, although its super star clusters may reach or exceed $\langle \Gamma \rangle \sim 1$ on small scales (Krumholz & Matzner 2009; Murray et al. 2010, 2011).

While this work has yielded useful insights, it has been limited to examining the mean properties of star-forming systems. However, the real ISM is far from uniform. An important outstanding question is how momentum injection — whether deposited by radiation pressure on dust, supernova explosions, or other processes — couples to a supersonically turbulent ISM or GMC. Here, we highlight an important piece of physics: over a broad range of parameters, the Eddington luminosity per unit mass (L_{Edd}/M ; in the case of radiation pressure) or the critical momentum input rate to expel gas (\dot{P}_{Edd}/M ; in the case of supernovae or stellar winds) is linearly proportional to the surface density of gas Σ along any line of sight. For a medium with average gas surface density $\langle \Sigma \rangle$, one might imagine that if the actual luminosity L or momentum injection rate P is below $\langle L_{\text{Edd}} \rangle$ or $\langle \dot{P}_{\text{Edd}} \rangle$ that no material is ejected. However, since the medium is supersonically turbulent, the momentum sources “see” a broad lognormal probability distribution function (PDF) of surface densities whose width is controlled by the Mach number of the turbulence. At sufficiently low Σ , the medium will thus be super-Eddington. Setting the Σ -dependent Eddington ratio to unity defines a critical surface density Σ_{crit} . The material in sightlines with $\Sigma < \Sigma_{\text{crit}}$ will be accelerated to the local escape velocity (or above) in a local dynamical timescale (or less).

We develop this model here. We argue that the gas along sightlines with $\Sigma < \Sigma_{\text{crit}}$ is ejected. The mechanism is generic in the sense that any turbulent medium with momentum sources should be unstable to some mass loss. In practice, we show that because of the shape of the surface density and mass PDFs the system needs to be within about 1/10th of the Eddington limit for significant gas expulsion, with the degree of mass loading determined by the Mach number of the turbulence and the ratio $\Sigma_{\text{crit}}/\langle \Sigma \rangle$.

In the context of radiation pressure on dust, a handful of studies have previously considered the interaction between radiation forces and a turbulent medium, and these have focused on the highly optically-thick limit applicable to surface densities larger than $\sim 10^4 M_{\odot} \text{ pc}^{-2} \sim 0.5 \text{ g cm}^{-2} \sim 10^{23} \text{ cm}^{-2}$, where the reradiated FIR emission might be trapped by the dusty gas. These works include both semi-analytic calculations with model turbulent column density PDFs (Murray et al. 2010; Hopkins et al. 2011) and full numerical radiation hydrodynamics (Krumholz & Thompson 2012, 2013; Davis et al. 2014; Skinner & Ostriker 2015) to assess whether the effective momentum coupling optical depth is in fact as large as the average FIR optical depth in a turbulent medium with lower column density sightlines. The general result of these studies is that the actual momentum deposition is smaller than what one would guess for a laminar, non-turbulent medium, though the extent of the deviation is still uncertain. We note that in the FIR optically-thick limit, Davis et al. (2014) (their Section 5.2) discussed the possibility that radiation pressure might launch outflows from galaxies that are below the average Eddington limit by having enhanced fluxes in lower-column density channels driven by the radiation Rayleigh-Taylor instability. Similar numerical calculations applicable to the broad column density regime where $L_{\text{Edd}}/M \propto \Sigma$, and where the effect highlighted in this paper

generally find that $\text{SFR}/\text{Area} \propto \Sigma^x$ with $x < 2$ (e.g., $x \simeq 1.4$; Kennicutt 1998). See Section 3.1.

should apply have yet to be undertaken in the galaxy feedback context.

In the supernova context, Shetty & Ostriker (2012) and Martizzi et al. (2014) have explored how the momentum deposition couples to and regulates the turbulent ISM, but neither global outflows nor GMC disruption were the focus of their work. Hopkins et al. (2012) explored the development of winds in full galaxy simulations with both radiation pressure and supernova feedback, and in principle, if turbulence was well-resolved on the scales of individual GMCs, we would expect the effect identified here to be present in their calculations. However, in their simulations it is difficult to disentangle the effects of supernovae, which were treated with full hydrodynamics, from the effects of radiation pressure, which were handled via sub-grid model analogous to the semi-analytic treatments discussed above. Creasey et al. (2013) follow the development of outflows in a supernova-driven ISM with energy deposition and momentum. A structured turbulent ISM was also part of Cooper et al. (2008)’s calculation of the superwind from M82. As we discuss in Section 3.3, the ram pressure acceleration of low-column density sightlines ($\Sigma < \Sigma_{\text{crit}}$) by either a hot wind produced by energy injection from supernovae or the direct momentum injection can also be interpreted in terms of an Eddington limit. The former point was recently explored by Zhang et al. (2015).

In Section 2 we discuss the Eddington limit for momentum input in a medium of given surface density. In Section 2.2 we compute the PDF of area and mass for a vertically-averaged supersonically turbulent medium and calculate the interaction of momentum sources with this medium. In Section 3 we provide a discussion of our results, with applications to the ISM of galaxies and GMCs, and other momentum sources. Section 4 provides a brief conclusion.

2 THE EDDINGTON LIMIT IN DRIVEN SUPERSONIC TURBULENCE

2.1 The Single-Scattering Eddington Limit

We start by considering a spherical source of UV/optical luminosity L and mass M surrounded by a turbulent dusty medium. Our arguments can be generalized to a thin disk geometry or other momentum sources. The medium surrounding the source has an area-averaged gas surface density $\langle \Sigma \rangle$, but presents a distribution of surface densities to the central source because it is turbulent. The equation of motion for gas along any line of sight with surface density Σ that is optically-thick to the incoming emission but optically-thin to the reradiated FIR is

$$\frac{dv}{dt} = -\frac{GM}{r^2} + \frac{L}{4\pi r^2 c} \frac{1}{\Sigma}, \quad (1)$$

which implies an Eddington luminosity of

$$\frac{L_{\text{Edd}}}{M} \simeq 4\pi Gc\Sigma \simeq 130 \frac{L_{\odot}}{M_{\odot}} \Sigma_{0.01}, \quad (2)$$

where $\Sigma_{0.01} = \Sigma/0.01 \text{ g cm}^{-2}$ and $0.01 \text{ g cm}^{-2} \simeq 50 M_{\odot} \text{ pc}^{-2} \simeq 6 \times 10^{21} \text{ cm}^{-2}$. The Eddington ratio along the line of sight is then

$$\Gamma(\Sigma) = \frac{L}{L_{\text{Edd}}(\Sigma)}, \quad (3)$$

where we explicitly note the functional dependence of Γ on Σ . In the case of an arbitrary momentum source \dot{P} , one can substitute

$L/c \rightarrow \dot{P}$ in the above. Recent work by Faucher-Giguere et al. (2013) implies that the net momentum injection rate from supernovae might be as much as $\dot{P}_{\text{SNe}} \sim 10L/c$. We return to this issue in Section 3.

In the context of radiation pressure, note that equation (1) is valid over about 2.5 dex in Σ . For $\Sigma \lesssim 1/\kappa_{\text{UV}} \simeq 10^{-3} \kappa_{\text{UV},3}^{-1} f_{\text{dg},\text{MW}}^{-1} \text{ g cm}^{-2}$ — where $\kappa_{\text{UV},3} = \kappa_{\text{UV}}/10^3 \text{ cm}^2 \text{ g}^{-1}$ is a typical UV continuum dust opacity and $f_{\text{dg},\text{MW}}$ is the dust-to-gas ratio scaled to the Milky Way value — the medium becomes optically-thin to the incident UV radiation and $1/\Sigma$ should be replaced by κ_{UV} in equation (1). Conversely, for $\Sigma \gtrsim 1/\kappa_{\text{IR}} \simeq 0.2 \kappa_{\text{IR},0.7}^{-1} f_{\text{dg},\text{MW}}^{-1} \text{ g cm}^{-2}$, where κ_{IR} is the Rosseland-mean opacity (e.g., Semenov et al. 2003), the medium becomes optically thick to the reradiated IR and $1/\Sigma$ should be replaced by κ_{IR} in equation (1). However, as discussed by many authors (see, e.g., Krumholz & Matzner 2009; Murray et al. 2010; Krumholz & Thompson 2012, 2013; Davis et al. 2014), it is unclear if the momentum coupling in the optically-thick limit translates into a momentum input as large as $\tau_{\text{IR}} = \kappa_{\text{IR}} \Sigma$ in a turbulent medium. Here, we focus on the range of parameters where the single-scattering limit applies and return to a discussion of the IR optically-thick and UV optically-thin regimes in Section 3.

If the turbulent dusty medium has an average gas surface density $\langle \Sigma \rangle$, the average Eddington luminosity is simply

$$\langle L_{\text{Edd}} \rangle = 4\pi GMc \langle \Sigma \rangle. \quad (4)$$

From equation (2) we then see that for source luminosity L , there is then a critical surface density below which $\Gamma \geq 1$:

$$\frac{\Sigma_{\text{crit}}}{\langle \Sigma \rangle} = \frac{L}{\langle L_{\text{Edd}} \rangle} \equiv \langle \Gamma \rangle. \quad (5)$$

All regions exposed to the central source with $\Sigma < \Sigma_{\text{crit}}$ will be accelerated out of the local gravitational potential by momentum deposition. Solving equation (1) we find the classic result that

$$\frac{v(r)}{v_{\text{esc}}(R_0)} = \left(1 - \frac{R_0}{r}\right) [\Gamma(\Sigma) - 1]^{1/2}, \quad (6)$$

where $v_{\text{esc}} = (2GM/R_0)^{1/2}$, R_0 is the initial radius of the medium, and where we have assumed that Σ is constant with radius as the cloud is accelerated. In this limit, for $r \gg R_0$, $v_{\infty} \simeq v_{\text{esc}}(R_0)(\Gamma - 1)^{1/2}$ and the asymptotic velocity is tied to the escape velocity from the central source. If the ejected medium instead expands as it is accelerated so that the angle subtended by the cloud from the source does not decrease as r^{-2} , then the cloud may reach much higher velocity (Thompson et al. 2014). In the context of radiation pressure on dust, if the cloud subtends a constant solid angle as it is accelerated, its asymptotic velocity is $v_{\infty} \simeq (R_{\text{UV}} L / (M_{\text{cloud}} c))^{1/2}$ if $R_{\text{UV}} \gg R_0$, where M_{cloud} is the mass of the cloud and $R_{\text{UV}} = (\kappa_{\text{UV}} M_{\text{cloud}} / 4\pi)^{1/2}$ is the radius at which the cloud becomes optically thin to the incident UV radiation. This assumes that the source L is constant on the timescale needed to reach R_{UV} , which is unlikely in the case of an intervening turbulent medium. We return to this issue in Section 2.2.

Taking equation (6) at face value, the acceleration time on a scale R_0 is then

$$t_{\text{acc}}(\Sigma) = \left(\frac{R_0^3}{2GM}\right)^{1/2} [\Gamma(\Sigma) - 1]^{-1/2}. \quad (7)$$

2.2 Interaction with a Turbulent Medium

In a turbulent medium, the sources of luminosity see a broad distribution of column densities along each line of sight, and the fraction of mass that finds itself super-Eddington will depend on this distribution. A number of numerical experiments have found that, for supersonic isothermal turbulence, the probability distribution function (PDF) of column densities is well-approximated by a lognormal distribution (Ostriker et al. 2001; Vázquez-Semadeni & García 2001; Federrath et al. 2010)

$$p_{\pm}(x) = \frac{1}{(2\pi\sigma_{\ln\Sigma}^2)^{1/2}} \exp\left[-\frac{(x - \bar{x})^2}{2\sigma_{\ln\Sigma}^2}\right] \quad (8)$$

where $x = \ln(\Sigma/\langle\Sigma\rangle)$. Conservation of mass requires that the mean \bar{x} and dispersion $\sigma_{\ln\Sigma}$ be related by $\bar{x} = \mp\sigma_{\ln\Sigma}^2/2$. The quantity $p_+(x)$ gives the areal PDF (i.e., the probability of measuring a certain column density if one chooses a line of sight passing through a random position), while $p_-(x)$ gives the mass PDF (i.e., the probability of measuring a certain column density if one chooses a line of sight passing through a random mass element).

The dispersion of the lognormal $\sigma_{\ln\Sigma}$ is related to the Mach number of the turbulence. For volume density, which is also well-described by a lognormal, numerous authors have found that the non-magnetized turbulence with mixed forcing produces a dispersion

$$\sigma_{\ln\rho}^2 \approx \ln(1 + \mathcal{M}^2/4) \quad (9)$$

in the log density PDF, where \mathcal{M} is the three-dimensional Mach number of the turbulence (e.g., see the recent review by Krumholz 2014). The dispersion of the column density PDF is smaller due to averaging over the line of sight, but the relationship has been subject to significantly less exploration in numerical simulation than that between \mathcal{M} and the dispersion of the volume density PDF. To estimate the dispersion of the column density PDF, we follow an approach suggested by Brunt et al. (2010a,b). They consider a periodic box of size L , and show that the ratio of the dispersions of column density, σ_{Σ} , and volume density, σ_{ρ} , are related by

$$R \equiv \left(\frac{\sigma_{\Sigma}}{\sigma_{\rho}}\right)^2 = \frac{\sum_{k_x, k_y = -\infty}^{\infty} P(k_x, k_y, 0) - P(0, 0, 0)}{\sum_{k_x, k_y, k_z = -\infty}^{\infty} P(k_x, k_y, k_z) - P(0, 0, 0)}, \quad (10)$$

where $P(k_x, k_y, k_z)$ is the power spectral density of the density field at point (k_x, k_y, k_z) in Fourier space, and the wave vectors (k_x, k_y, k_z) are normalized such that $k_x = 1$ corresponds to a mode with wavelength $\lambda = 2L$, i.e., $k_x = 1$ is the largest mode that will fit in the box. Note that these are dispersions of the column and volume densities themselves, not of their logarithms. For a lognormal PDF, the dispersions of the density and its logarithm are related by

$$\sigma_{\ln\rho}^2 = \ln(1 + \sigma_{\rho}^2), \quad (11)$$

and similarly for the column density. Combining the previous three equations, we have

$$\sigma_{\ln\Sigma}^2 \approx \ln(1 + R\mathcal{M}^2/4). \quad (12)$$

The value of R depends on the shape of the density power spectrum. For homogenous isotropic turbulence $P(k_x, k_y, k_z)$ must depend on $k = (k_x^2 + k_y^2 + k_z^2)^{1/2}$ alone, and several numerical studies have found that the relationship is reasonably well-described by a power law $P(k) \propto k^{-\alpha}$ with an index α that depends on the Mach number of the turbulence, and varies from

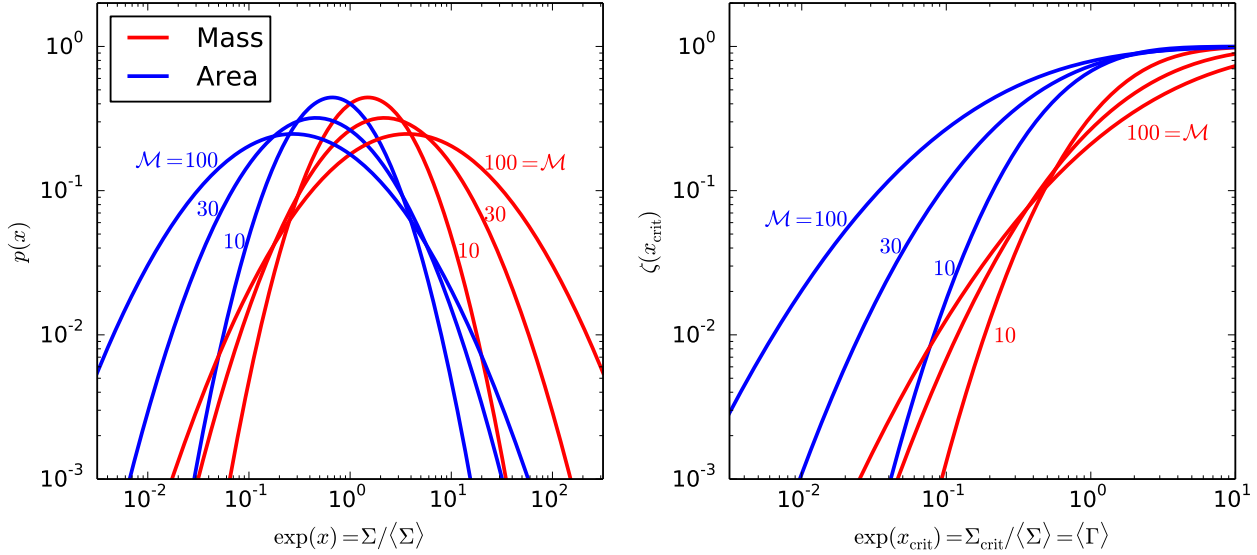


Figure 1. *Left:* The areal column density probability distribution function (PDF) (blue; $p_+(x)$) and the mass column density PDF (red; $p_-(x)$) as given in equation 8, as a function of $e^x = \Sigma/\langle\Sigma\rangle$ for Mach numbers $\mathcal{M} = 10, 30$, and 100 . This plot shows that the areal (mass) PDF is peaked below (above) the mean value of the column density, and that it broadens as \mathcal{M} increases. *Right:* The integral of the areal (blue; ζ_+) and mass (red; ζ_-) PDFs from $x = -\infty$ to x_{crit} (eq. 15), as given in eq. 16, as a function of the average Eddington ratio $\exp(x_{\text{crit}}) = \langle\Gamma\rangle$. This panel shows that for a system with $\langle\Gamma\rangle = 0.1$ and $\mathcal{M} \gtrsim 30$ that $\gtrsim 10\%$ ($\zeta_+ \gtrsim 0.1$) of the area and $\gtrsim 1\%$ ($\zeta_- \gtrsim 10^{-2}$) of the mass is super-Eddington.

$\alpha \approx 3.7$ at near-transonic turbulence to $\alpha \approx 2.5$ for $\mathcal{M} \gg 1$ (Kim & Ryu 2005; Beresnyak et al. 2005; for a summary and references to further results, see the review by Krumholz 2014). Since most of the astrophysical systems with which we are concerned have $\mathcal{M} \gg 1$, we adopt $\alpha = 2.5$ as our fiducial value. This power law behavior of $P(k)$ must stop at sufficiently high k for the dispersion to remain finite, and the natural truncation scale is the sonic length scale, below which the turbulence becomes subsonic and is thus no longer able to drive density fluctuations (Krumholz & McKee 2005); in our normalized wave vector units, this scale corresponds to $k = \mathcal{M}^2$. We therefore adopt as an *ansatz* that

$$P(k) \propto \begin{cases} 0, & k = 0 \\ k^{-\alpha}, & 1 \leq k \leq \mathcal{M}^2 \\ 0, & k > \mathcal{M}^2 \end{cases}. \quad (13)$$

With this *ansatz*, and approximating the sums in equation (10) by integrals (appropriate for $\mathcal{M} \gg 1$), we have

$$R = \frac{1}{2} \left(\frac{3 - \alpha}{2 - \alpha} \right) \left[\frac{1 - \mathcal{M}^{2(2-\alpha)}}{1 - \mathcal{M}^{2(3-\alpha)}} \right]. \quad (14)$$

By using this value of R in equation (12) we have completed the specification of the PDF of Σ in terms of \mathcal{M} .

Now we are in a position to ask how much mass and area is contained in regions where Σ is small enough for the gas to be super-Eddington. We define a critical value of x for this condition to be satisfied as (see eq. 5)

$$x_{\text{crit}} = \ln[\Sigma_{\text{crit}}/\langle\Sigma\rangle]. \quad (15)$$

Integrating $p_{\pm}(x)$ from $x = -\infty$ to $x = x_{\text{crit}}$ yields the total fraction of the area and mass, respectively, of the medium with $\Sigma <$

$\Sigma_{g, \text{crit}}$:

$$\begin{aligned} \zeta_{\pm}(x_{\text{crit}}) &= \int_{-\infty}^{x_{\text{crit}}} p_{\pm}(x) dx \\ &= \frac{1}{2} \left[1 \pm \text{erf} \left(\frac{\pm 2x_{\text{crit}} + \sigma_{\ln \Sigma}^2}{2\sqrt{2}\sigma_{\ln \Sigma}} \right) \right]. \end{aligned} \quad (16)$$

In the right hand panel of Figure 1 we plot $\zeta_{\pm}(x_{\text{crit}})$ for the area (blue) and the mass (red), respectively, for $\mathcal{M} = 10, 30$, and 100 . For $\langle\Gamma\rangle \simeq 0.1$ and $\mathcal{M} = 30$, we see that $\zeta_- \sim 10^{-2}$ and $\zeta_+ \sim 0.2$, implying that about 1% of the mass and 20% of the area of the system would be super-Eddington.

An important question is whether the matter along a super-Eddington line of sight can be accelerated before the turbulence “erases” the local conditions. If the column density field fluctuates in a time much less than the time to accelerate the matter, we expect no material to be ejected. The relevant comparison is then the ratio $t_{\text{acc}}(\Sigma)/t_{\text{cross}}(\lambda)$, where t_{acc} is given by equation (7) and $t_{\text{cross}}(\lambda) \sim \lambda/\delta v(\lambda)$ is the crossing time of the turbulence with velocity $\delta v(\lambda)$ to cross a scale λ over which Σ obtains:

$$\frac{t_{\text{acc}}(\Sigma)}{t_{\text{cross}}(\lambda)} \sim \left(\frac{\delta v(\lambda)}{v_{\text{esc}}(R_0)} \right) \left(\frac{R_0}{\lambda} \right) \frac{1}{[\Gamma(\Sigma) - 1]^{1/2}}, \quad (17)$$

where $v_{\text{esc}}(R_0) = (2GM/R_0)^{1/2}$. To our knowledge, the projected persistence time of low column density structures in simulations of highly supersonic turbulence has not been reported in the literature. However, in the GMC context on the largest scales ($\lambda \sim R_0$), we expect $\delta v \sim v_{\text{esc}}$, implying that $t_{\text{acc}}(\Sigma) < t_{\text{cross}}(R_0)$ if $\Gamma(\Sigma) \gtrsim \text{few}$. A similar conclusion is reached by considering a geometrically thin disk with flux F and total surface density Σ_{tot} on a scale height h . We thus conclude that for $\Gamma(\Sigma)$ larger than ~ 2 , the material should be accelerated before turbulence erases the local conditions. In the GMC context, the material is accelerated to the escape velocity, whereas for a geometrically thin disk the super-

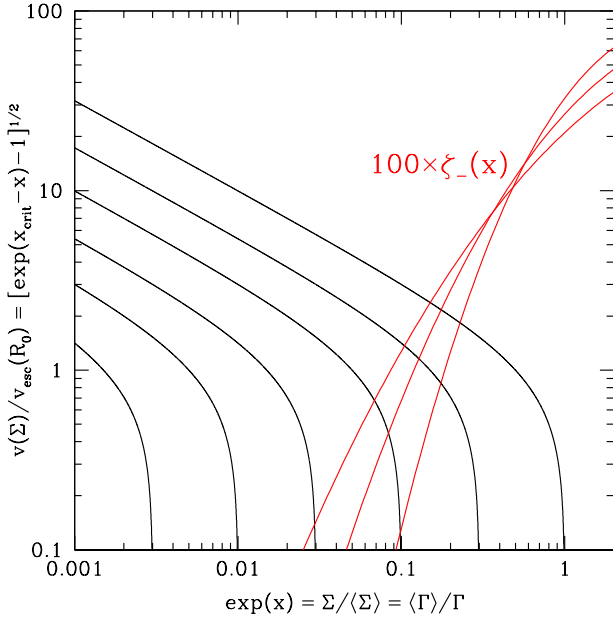


Figure 2. Velocity distribution $v(\Sigma)/v_{\text{esc}}(R_0)$ (black lines) of ejected material as a function of $e^x = \Sigma/\langle\Sigma\rangle = \langle\Gamma\rangle/\Gamma$ for $\langle\Gamma\rangle = 3 \times 10^{-2}$, 0.01, 0.03, 0.1, 0.3, and 1 (lowest to highest). The red lines show $100\zeta_-(x)$ from Figure 1 (right panel) for $\mathcal{M} = 10, 30$, and 100. See equation (18).

Eddington matter will be accelerated to a characteristic velocity of $v^2 \sim \pi G \Sigma_{\text{tot}} h$, the vertical velocity dispersion of the gas.²

If the material with $\Sigma < \Sigma_{\text{crit}}$ is ejected, and if the surface density of the ejected regions is constant as a function of radius in its first dynamical time as it is accelerated, then the velocity distribution is just

$$\frac{v(\Sigma)}{v_{\text{esc}}(R_0)} \simeq \left(\frac{\Sigma_{\text{crit}}}{\Sigma} - 1 \right)^{1/2} = \left[e^{(x_{\text{crit}} - x)} - 1 \right]^{1/2}. \quad (18)$$

Figure 2 shows v/v_{esc} as a function of e^x for a wide range of $\langle\Gamma\rangle$ from $3 \times 10^{-2} - 1$ (black solid lines, lowest to highest). The red lines show the integral of the mass PDF times 100 ($100\zeta_-(x)$) from the right panel of Figure 1. We see that only a very small amount of mass can reach $v/v_{\text{esc}} \gg 1$ in a single dynamical time on scale R_0 . For example, taking $\langle\Gamma\rangle = 0.1$, a fraction $\sim 10^{-2}$ ($100\zeta_- \simeq 1$) of the mass reaches $v/v_{\text{esc}} \sim 1$ for $\mathcal{M} = 100$, but only $\lesssim 10^{-3}$ reaches $v/v_{\text{esc}} \gtrsim 2$ because of the very strong drop in $\zeta_-(x)$. Taking $\langle\Gamma\rangle = 1$, more than 0.02 of the gas mass reaches $v/v_{\text{esc}} \gtrsim 2$, whereas a fraction 0.001 reaches $v/v_{\text{esc}} \gtrsim 6$.

3 DISCUSSION

In Section 3.1 we first discuss the application of our results to observed star-forming galaxies as a whole in the context of radiation pressure. For nominal CO-H₂ conversion factors these systems are on average below the single-scattering Eddington limit (Andrews

² This follows from solving the one-dimensional planar momentum equation for a column of gas being accelerated out of a thin disk (see eq. 1), or by equating $\rho v^2/2 \sim \pi G \Sigma_{\text{tot}}^2$ in hydrostatic equilibrium and noting $\Sigma_{\text{tot}} = 2\rho h$.

& Thompson 2011). Because in a thin disk geometry we expect low-column sightlines that are near the Eddington limit to be accelerated to only of order the vertical velocity dispersion of the gas ($\sim 10 - 50 \text{ km s}^{-1}$ for most systems) the importance of radiation pressure alone as a momentum injection mechanism is likely not dramatic for most systems. Even so, some galaxies do have average Eddington ratios closer to unity than others, and in all galaxies some gas will be in low-column density sightlines that are effectively strongly super-Eddington. In addition, we find that our results depend sensitively on both the CO-H₂ conversion factor and the total momentum injection rate, which may be contributed to by other momentum sources (see Section 3.3).

The application to massive star-forming sub-regions within galaxies is given in Section 3.2. Even $z \sim 0$ galaxies may reach the single-scattering radiation pressure Eddington limit (Krumholz & Matzner 2009; Murray et al. 2010, 2011), driving shells vertically out of the plane of galaxies at relatively high velocity (Fig. 2), and our results indicate the star-formation efficiency in GMCs may be substantially modified by the interaction of radiation pressure with the turbulent medium.

3.1 Application to Galaxies

In a galactic disk with a continuous star formation rate per unit area $\dot{\Sigma}_*$, the flux produced by the newborn stars will be $F \approx \epsilon \dot{\Sigma}_* c^2$, where $\epsilon \simeq 7 \times 10^{-4}$ is an IMF-dependent constant. This can be compared to the Eddington flux, which is

$$F_{\text{Edd}} = 2\pi G c f_g^{-1} \Sigma_g^2, \quad (19)$$

where Σ_g is the gas surface density and f_g is the gas mass fraction. We therefore have

$$e^{x_{\text{crit}}} = \frac{F}{F_{\text{Edd}}} = \left(\frac{\epsilon c f_g}{2\pi G} \right) \frac{\dot{\Sigma}_*}{\Sigma_g^2}. \quad (20)$$

Loci of constant F/F_{Edd} therefore correspond to relationships $\dot{\Sigma}_* \propto \Sigma_g^2$ between galaxies' star formation rate and gas content (at fixed f_g ; see, e.g., Andrews & Thompson 2011). Conversely, for any observed galaxy for which Σ_g and $\dot{\Sigma}_*$ are known, and for which f_g is known or measured, we can use equation (20) to infer x_{crit} and thence ζ , the fraction of mass that is super-Eddington.

In Figure 3 we show loci of constant F/F_{Edd} assuming a constant gas fraction of $f_g = 0.3$ in the $\Sigma_g - \dot{\Sigma}_*$ plane overlaid with data for a large collection of local and high-redshift star-forming galaxies taken from the compilation of Krumholz (2014). For the assumed f_g , observed galaxies fall below $F = F_{\text{Edd}}$, and most fall below $F = F_{\text{Edd}}/10$. There is a systematic trend whereby higher star formation rate galaxies have lower values of F/F_{Edd} , which is simply a consequence of the fact that constant F/F_{Edd} would require that the star formation rate rise with gas surface density as $\Sigma_g \propto \Sigma_*^2$ (e.g., Thompson et al. 2005; Andrews & Thompson 2011), and the observed relationship between gas content and star formation is apparently not quite that steep.

In Figure 4, we show the implications of these results for ζ , the fraction of mass that is expected to be super-Eddington, and the mass-loading rate. We parameterize the star formation rate per unit area as

$$\dot{\Sigma}_* = \epsilon_{\text{ff}} \Sigma_g / t_{\text{ff}}, \quad (21)$$

where t_{ff} is the free-fall time at the average density of the star-forming gas and ϵ_{ff} is an efficiency factor. If we adopt as an *ansatz*

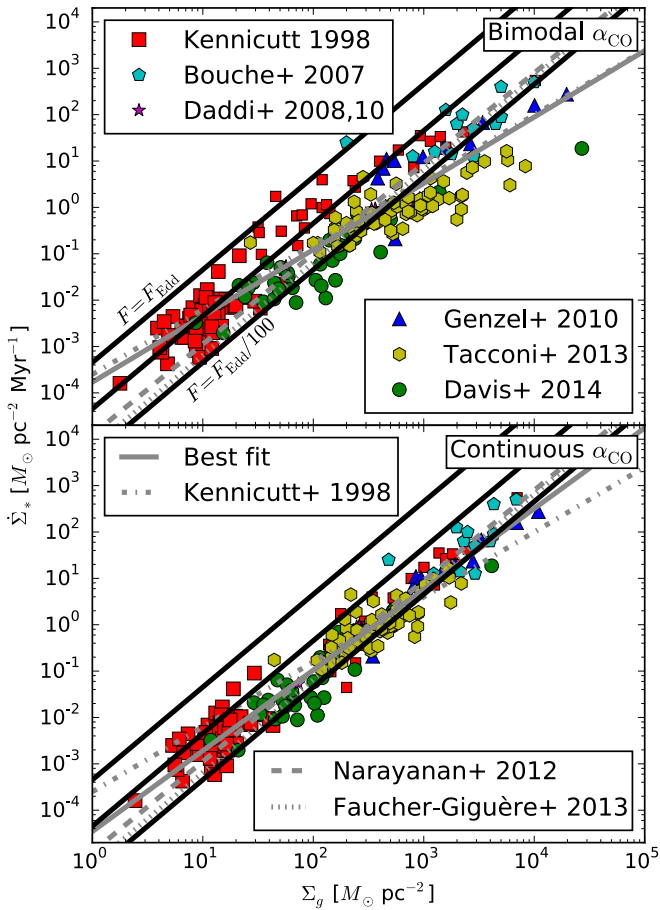


Figure 3. Locations of observed galaxies, together with theoretical curves, in the $\Sigma_g - \dot{\Sigma}_*$ plane. Black lines show the locations for $F = F_{\text{Edd}}$, $F = F_{\text{Edd}}/10$, and $F = F_{\text{Edd}}/100$, as indicated; these curves were computed for $f_g = 0.3$, and their vertical position varies as f_g^{-1} . Points indicate a compilation of data on observed galaxies taken from Krumholz (2014). Original sources for the data are as follows: Kennicutt (1998), Bouche et al. (2007), Daddi et al. (2008) and Daddi et al. (2010a), Genzel et al. (2010), Tacconi et al. (2013), and Davis et al. (2014). Gray curves indicate a least squares fit to this data set (solid), the Kennicutt (1998) relation (dot-dashed), and fits by Narayanan et al. (2012) (dashed) and Faucher-Giguère et al. (2013) (dot-dashed) to subsets of the data shown, and using a variety of models for α_{CO} (see also Ostriker & Shetty 2011). Finally, the upper panel shows the results using the bimodal α_{CO} values recommended by Daddi et al. (2010b), while the bottom panel uses the theoretical α_{CO} value computed by Narayanan et al. (2012).

that the wind mass ejection rate is given roughly by

$$\dot{\Sigma}_{\text{wind}} = \zeta(x_{\text{crit}})\Sigma_g/t_{\text{ff}}, \quad (22)$$

this implies that the mass loading factor

$$\eta \equiv \frac{\dot{\Sigma}_{\text{wind}}}{\dot{\Sigma}_*} = \frac{\zeta}{\epsilon_{\text{ff}}}. \quad (23)$$

Figure 4 shows η for the galaxies in the sample of Figure 3 with a fiducial choice of $\epsilon_{\text{ff}} = 0.01$. Our values of ζ , which range from $\sim 10^{-4} - 10^{-1}$, coupled with our choice of ϵ_{ff} on galactic scales, imply mass loading factors of $\sim 10^{-3} - 10$. Figure 4 suggests that the direct single-scattering radiation pressure may be a major con-

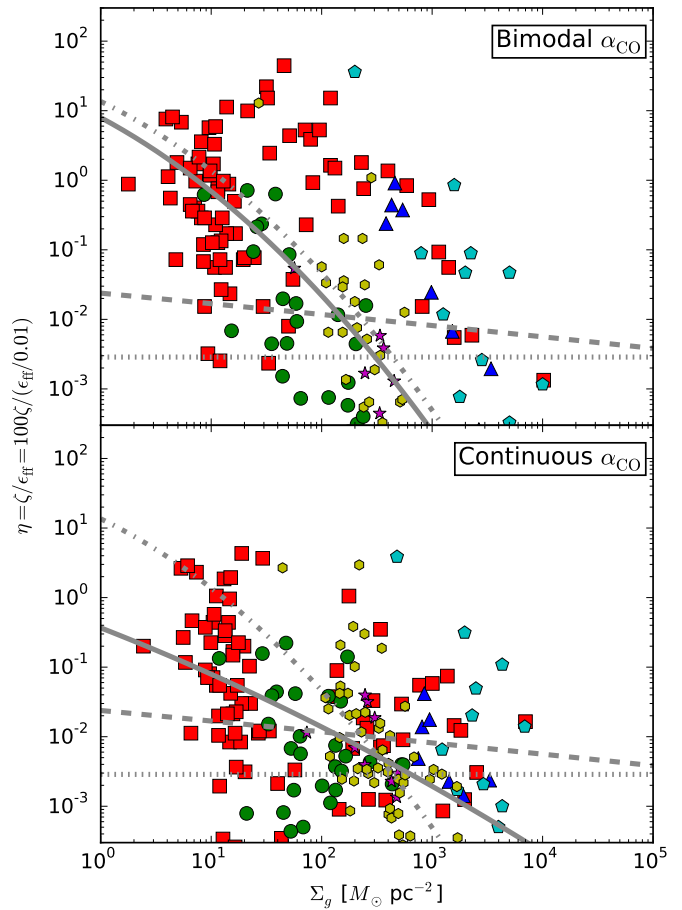


Figure 4. Values of ζ , the fraction of the mass that is super-Eddington, versus gas surface density Σ_g . Data points are identical to those shown in Figure 3, and gray lines are for the same fits as in that Figure: the best-fit to the full data set (solid) the Kennicutt (1998) relation (dot-dashed), and the fits by Narayanan et al. (2012) (dashed) and Faucher-Giguère et al. (2013) (dot-dashed). As in Figure 3, in the upper panel the observed galaxies have surface densities assigned using the Daddi et al. (2010b) bimodal α_{CO} , while in the lower panel surface densities are computed using the theoretical α_{CO} of Narayanan et al. (2012). All calculations are done for a Mach number $\mathcal{M} = 30$ and $\alpha = 2.5$ for the slope of the density power spectrum in equation (13). Different choices change the results quantitatively but not qualitatively.

tributor to the mass loading on galactic scales for some galaxies with mean surface densities $\lesssim 100 M_{\odot} \text{pc}^{-2}$. For galaxies with higher surface densities the effects of radiation pressure are systematically smaller because the surface density does not rise with star formation rate quickly enough to keep F/F_{Edd} from falling (Andrews & Thompson 2011). Since ζ is exponentially sensitive to F/F_{Edd} , even a modest fall translates to a dramatic reduction in the mass-loading factor.³

³ At high surface densities, the effects of large FIR optical depth and the reprocessed radiation may increase the importance of radiation pressure in dense starbursts or their FIR optically-thick star-forming sub-regions, but we do not focus on this regime. See Thompson et al. (2005); Andrews & Thompson (2011); Murray et al. (2010); Krumholz & Thompson (2012, 2013); Davis et al. (2014); Skinner & Ostriker (2015).

Note that the choice of ϵ_{ff} directly impacts the inferred mass-loading factor η , and for this reason we explicitly label the ordinate of Figure 4 with the ϵ_{ff} dependence. Since we assume radiation pressure acts on local scales in individual star forming regions, we adopt a constant value for ϵ_{ff} inferred from the free-fall time for the average of the star-forming molecular clouds on large scales (Krumholz 2014). We extend this to feedback within GMCs with varying ϵ_{ff} in Section 3.2. Note that our working definition of ϵ_{ff} in Figure 4 is different from the one used by Faucher-Giguere et al. (2013) who evaluate the free-fall time at the average ISM density (typically significantly lower than the average density of star-forming clouds) and argue both that some galaxies have $\epsilon_{\text{ff}} \gtrsim 0.1$, and that rather than being constant, ϵ_{ff} scales with gas fraction and circular velocity.

We caution that the results presented are also sensitive to the choice of the factor α_{CO} used to convert between observable CO emission and surface density of molecular gas, particularly because of the exponential dependence of ζ on F/F_{Edd} . To illustrate this, the top panels of Figures 3 and 4 show the data where we have inferred gas surface densities using the values of α_{CO} suggested by Daddi et al. (2010b): $\alpha_{\text{CO}} = 4.6 M_{\odot} (\text{K km s}^{-1} \text{pc}^{-2})^{-1}$ for local non-starburst galaxies, $\alpha_{\text{CO}} = 3.6 M_{\odot} (\text{K km s}^{-1} \text{pc}^{-2})^{-1}$ for high- z disk galaxies, and $\alpha_{\text{CO}} = 0.8 M_{\odot} (\text{K km s}^{-1} \text{pc}^{-2})^{-1}$ for starburst galaxies. The bottom panels show the exact same data but using the theoretical calibration of α_{CO} computed based on simulations and radiative transfer post-processing by Narayanan et al. (2011, 2012): $\alpha_{\text{CO}} = \min[6.3, 10.7 \langle W_{\text{CO}} \rangle^{-0.32}] / Z'^{0.65} (\text{K km s}^{-1} \text{pc}^{-2})^{-1}$, where $\langle W_{\text{CO}} \rangle$ is the observed CO line intensity in units of K km s^{-1} , Z' is the metallicity normalized to the Milky Way value, and we have used $Z' = 1$ for all galaxies.

The effect of using the theoretical α_{CO} calibration on the location of galaxies in the $\Sigma_g - \dot{\Sigma}_*$ plane is relatively modest, but it does lead to a somewhat steeper rise in $\dot{\Sigma}_*$ with Σ_g . Formally, the a linear least squares fit for the relation between Σ_g and $\dot{\Sigma}_*$ gives

$$\log \dot{\Sigma}_* = 1.43 \log \Sigma_g - 3.77 \quad (24)$$

for the Daddi et al. (2010b) α_{CO} , and

$$\log \dot{\Sigma}_* = 1.74 \log \Sigma_g - 4.46 \quad (25)$$

for Narayanan et al. (2011, 2012); in these formulae the gas surface densities are in units of $M_{\odot} \text{pc}^{-2}$ and the star formation rates are in units of $M_{\odot} \text{pc}^{-2} \text{Myr}^{-1}$, and the fits have been performed weighting all galaxies equally. Note that the slope of 1.74 we find using the Narayanan et al. calibration is shallower than the value of 1.95 found in the original Narayanan et al. paper. This is due to the significantly-expanded data set we make use of here. Using a variable α_{CO} , Ostriker & Shetty (2011) also found a relatively steep correlation: $\log \dot{\Sigma}_* = 1.9 \log \Sigma_g - 5.05$.

Although the change in slope between the two calibrations in equations (24) and (25) is only about 0.3, this has the effect of making ζ fall off much less dramatically with increasing Σ_g using the Narayanan et al. (2011, 2012) calibration rather than that from Daddi et al. (2010b). The difference is not enough to render radiation pressure significant in starbursts, but it is a reminder that a slope of 2 in the $\log \dot{\Sigma}_* - \log \Sigma_g$ relationship represents a critical value for momentum feedback models (Thompson et al. 2005; Andrews & Thompson 2011). Changes in the α_{CO} calibration severe enough to produce a star formation law with a slope of 2 appear unlikely based on current observations or theoretical models, but given the significant uncertainties can by no means be ruled out.

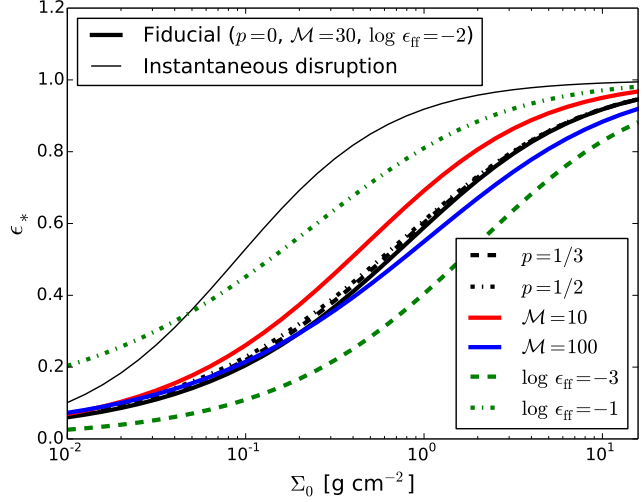


Figure 5. Final star formation efficiency ϵ_* versus starting surface density Σ_0 for our simple model of radiatively-driven mass loss. The black solid curve shows a fiducial set of parameters $p = 0$, $\mathcal{M} = 30$, and $\epsilon_{\text{ff}} = 0.01$, while the other curves show the results of varying one of these parameters.

3.2 Application to Giant Molecular Clouds

While the effects of radiation pressure alone may be fairly modest at galactic scales, they are much more significant at the scales of giant molecular clouds, which have much shallower potential wells than galaxies and proportionately higher star formation rates per unit mass. Consider a simple phenomenological model of a forming star cluster, somewhat similar to the models previously considered by Murray et al. (2010), Fall et al. (2010), and Dekel & Krumholz (2013): we start with a spherical ball of gas with an initial mass $M_g(0)$ and radius $R(0)$, containing no stars. At time $t = 0$ star formation begins, and thereafter occurs at a rate

$$\dot{M}_* = \epsilon_{\text{ff}} \frac{M_g}{t_{\text{ff}}}, \quad (26)$$

where M_g and t_{ff} are the instantaneous values of the gas mass and free-fall time.

The instantaneous stellar mass is M_* , and this stellar population produced a luminosity $L_* = \Psi M_*$, where $\Psi = 1140 L_{\odot} / M_{\odot}$ is the light to mass ratio of a zero-age stellar population with a standard IMF. Making the same *ansatz* as in the previous section, we estimate that the light from the newborn stars drives a wind out of the system with a mass flux

$$\dot{M}_w = \zeta(x_{\text{crit}}) M_g / t_{\text{ff}}, \quad (27)$$

where in this spherical geometry

$$\ln x_{\text{crit}} = \left(\frac{1 - f_g}{f_g} \right) \frac{\Psi}{4\pi G c \Sigma_{\text{tot}}}. \quad (28)$$

Here $f_g = M_g / (M_g + M_*)$ is the instantaneous gas fraction, and Σ_{tot} is the total gas plus stellar surface density. This last term will depend upon how the radius changes as star formation proceeds, and choose to parameterize this with a power law relationship, $R \propto [(M_* + M_g) / M_g(0)]^p$, where $p = 0$ corresponds to the gas-plus stellar cloud maintaining a constant radius, $p = 1/2$ to constant surface density, and $p = 1/3$ to constant volume density.

Consequently, the surface density Σ_{tot} evolves as

$$\Sigma_{\text{tot}} = \Sigma_0 \left(\frac{M_* + M_g}{M_g(0)} \right)^{1-2p}, \quad (29)$$

where $\Sigma_0 = M_g(0)/\pi R(0)^2$.

Dividing equations (26) and (27), we have

$$\frac{dM_w}{dM_*} = \eta = \frac{\zeta(x_{\text{crit}})}{\epsilon_{\text{ff}}}, \quad (30)$$

which we can easily integrate to obtain M_w as a function of M_* , where M_w is the mass ejected by winds up to the point where a mass M_* of stars has formed. The final star formation efficiency is simply

$$\epsilon_* = \frac{M_*}{M_g(0)} = \frac{M_*}{M_* + M_w} \quad (31)$$

evaluated at the point where $M_* + M_w = M_g(0)$, i.e., at the point where all the gas has been either converted to stars or lost to winds; ϵ_* is a function of the starting surface density Σ_0 , the Mach number \mathcal{M} of the turbulence, the index p describing how the radius changes as star formation proceeds, and the star formation rate per free-fall time ϵ_{ff} . However, only the first of these matters to any substantial degree. Figure 5 shows ϵ_* versus Σ_0 for a range of choices for other parameters. As the plot shows, a generic result is that star formation efficiencies of $\sim 50\%$ are reached at surface densities of $\Sigma_0 \approx 1 \text{ g cm}^{-2}$; this is consistent with the findings of Fall et al. (2010), who used a much simpler model of mass loss that considered only explosive ejection of material and not steady winds as we have here. The thin solid line labelled “instantaneous disruption” assumes that the medium must come to the average Eddington limit before ejecting any mass and corresponds closely to the work of Murray et al. (2010). At typical surface densities of galactic giant molecular clouds, $\sim 0.03 \text{ g cm}^{-2}$ (Dobbs et al. 2014), the expected star formation efficiency is $\sim 10\%$, consistent with the low values typically found for such systems.

3.3 Other Momentum Injection Sources

In the application to whole galaxies, it is worth highlighting the potential importance of momentum injection by supernova explosions. Thompson et al. (2005) investigated the importance of momentum injection by supernovae in the ISM, and found them to be comparable to radiation pressure at high gas densities based on the work of Thornton et al. (1998). Recent reappraisals by Ostriker & Shetty (2011) and Faucher-Giguere et al. (2013) show that the net momentum input from supernovae can be as large as $\dot{P}_{\text{SNe}} \sim 10 - 20 \times L/c$, with a weaker gas density dependence (see also Martizzi et al. 2014). However, the calculation of the net momentum input to a turbulent medium from supernovae is likely less straightforward in an analytic approach than radiation pressure because the momentum of supernova explosions — the $10 - 20$ enhancement relative to L/c — is accumulated during the energy-conserving phase, as the remnants sweeps up mass. Individual parcels of gas with column density Σ (as in Section 2.1) will see a highly intermittent momentum injection rate. More work is needed to understand how the momentum injection rate from supernovae couples to the turbulent ISM (see, e.g., Kim et al. 2013). However, it is clear from the normalization of \dot{P}_{SNe} that it may dominate momentum input in galaxies and drive strong outflows: increasing the nominal momentum injection rate into galaxies by

a factor of $10 - 20$ would lower all of the black solid lines by the same factor in the left panels of Figure 4, making all galaxies near-Eddington and dramatically increasing their mass loading rates (right panels).

The ram pressure of a very hot thermal gas component, as in the wind model of Chevalier & Clegg (1985), may also deposit momentum in the medium. If the energy injection rate within a radius R is parameterized as $\dot{E}_{\text{hot}} = \alpha \dot{E}_{\text{SN}}$, where \dot{E}_{SN} is the energy injection rate of supernovae ($\sim 10^{51}$ ergs/100 yr, per M_{\odot} /yr of star formation) and if the hot gas mass outflow rate is $\dot{M}_{\text{hot}} = \beta \text{SFR}$, then the momentum injection rate for the hot gas at the surface of the star-forming medium is $\dot{P}_{\text{hot}} \simeq \dot{M}_{\text{hot}} V_{\text{hot}}$, where $V_{\text{hot}}(R) \simeq (2\dot{E}_{\text{hot}}/\dot{M}_{\text{hot}})^{1/2}$. Comparing this to the momentum injection rate from radiation pressure in the single-scattering limit yields $\dot{P}_{\text{hot}}/(L/c) \simeq 3(\alpha\beta)^{1/2} (7 \times 10^{-4}/\epsilon)$. For order unity $\alpha\beta$, as is inferred for the hot gas in the wind of M82 by Strickland & Heckman (2009), this momentum source may dominate radiation pressure, and, like \dot{P}_{SNe} , the contribution from \dot{P}_{hot} could shift the Eddington limit downward in Figure 4. Limits from X-ray observations indicate that $\beta \lesssim 1$ for $\text{SFR} \gtrsim 10 M_{\odot} \text{ yr}^{-1}$ galaxies (Zhang et al. 2014a), and numerical calculations indicate that both α and β may be functions of the gas surface density of galaxies (Creasey et al. 2013).

Other momentum injection sources include stellar winds and cosmic rays. The former is expected to be significantly less important than supernovae in a time-averaged stellar population in galaxies (Leitherer et al. 1999), but may well be important in the early-time disruption of GMCs before any supernovae have occurred. Estimates for the momentum input from cosmic rays indicate that they may also dominate radiation pressure in normal galaxies and possibly starbursts, depending on the CR scattering mean free path, the cosmic ray pion production rate, and — of specific relevance for this work — how the CRs interact and dynamically couple to low-column density regions in a turbulent ISM (Ptuskin et al. 1997; Socrates et al. 2008; Jubelgas et al. 2008; Lacki et al. 2011; Hanasz et al. 2013).

4 CONCLUSIONS

The Eddington luminosity per unit mass for gas subject to a momentum source is proportional to the column density of the medium. Because turbulent media present a broad column density distribution to the momentum sources, there exists a critical column density below which the medium is super-Eddington. Even systems that are sub-Eddington will have super-Eddington sightlines.

We have developed this idea using a simple formalism and discussed some of the implications for observed galaxies (Fig. 4) and the star formation efficiency, evolution, and disruption of GMCs (Fig. 5). For average Eddington ratios of 0.1 and Mach numbers greater than about 30, we expect $\sim 1\%$ of the mass of the medium to be ejected per dynamical timescale (Fig. 1) with a well-defined velocity distribution (Fig. 2). This rate of mass ejection is comparable to the star formation efficiency per free-fall time when averaged on large scales and thus the instability we identify here may be relevant for ejecting gas even when the system is significantly below the average Eddington limit. An important uncertainty in our model is whether or not the projected persistence time of low column density structures in the tail of the column density PDF is shorter than

the dynamical timescale. This comparison of timescales directly affects whether material is ejected (Section 2.2), and should be investigated in multi-dimensional simulations.

We discuss a number of momentum sources in Section 3.3, but focus our discussion on radiation pressure in the single-scattering limit, which is likely most relevant for the early-time disruption of GMCs. Figure 3 shows the Eddington flux from normal galaxies and Figure 4 shows an estimate of their mass-loading factors η (eq. 23). For galaxies with gas surface densities less than $\sim 100 M_{\odot} \text{ pc}^{-2}$, we find a large scatter in η from $\sim 10^{-3} - 10$, indicating that radiation pressure feedback alone may be important for some galaxies. However, our results are highly sensitive to the assumed gas fraction and α_{CO} . On small scales, we compute the star formation efficiency in GMCs of specified initial gas surface density (Fig. 5).

The model is readily incorporated into subgrid and semi-analytic models of galaxies and/or GMC disruption. The addition of other momentum sources like supernovae, hot winds, and cosmic rays in such models remains the subject of future work, but the estimates of Section 3.3 suggest that they may be significant in driving material in low column-density super-Eddington sightlines out of star-forming galaxies and individual star-forming regions.

ACKNOWLEDGMENTS

We thank Eve Ostriker and Norm Murray for comments and Brant Robertson, Evan Scannapieco, Eliot Quataert, and Phil Hopkins for useful discussions. TAT thanks Chris Kochanek for a reading of the text. We gratefully acknowledge the Simons Foundation for funding the workshop *Galactic Winds: Beyond Phenomenology*, where this work was conceived. We also thank the Kavli Institute for Theoretical Physics and the organizers of *Gravity's Loyal Opposition: The Physics of Star Formation Feedback*, where a portion of this paper was written. This research was supported in part by the National Science Foundation under Grant No. PHY11-25915. TAT is supported in part by NASA Grant NNX10AD01G and NSF Grant 1516967. MRK is supported by NSF grants AST-0955300 and AST-1405962, NASA ATP grant NNX13AB84G, NASA TCAN grant NNX14AB52G.

REFERENCES

- Andrews, B. H., & Thompson, T. A. 2011, *ApJ*, 727, 97
 Beresnyak, A., Lazarian, A., & Cho, J. 2005, *ApJ*, 624, L93
 Bouché, N., Cresci, G., Davies, R., et al. 2007, *ApJ*, 671, 303
 Brunt, C. M., Federrath, C., & Price, D. J. 2010, *MNRAS*, 403, 1507
 —. 2010, *MNRAS*, 405, L56
 Chevalier, R. A., & Clegg, A. W. 1985, *Nature*, 317, 44
 Coker, C. T., Thompson, T. A., & Martini, P. 2013, *ApJ*, 778, 79
 Cooper, J. L., Bicknell, G. V., Sutherland, R. S., & Bland-Hawthorn, J. 2008, *ApJ*, 674, 157
 Creasey, P., Theuns, T., & Bower, R. G. 2013, *MNRAS*, 429, 1922
 Daddi, E., Bournaud, F., Walter, F., et al. 2010, *ApJ*, 713, 686
 Daddi, E., Dannerbauer, H., Elbaz, D., Dickinson, M., Morrison, G., Stern, D., & Ravindranath, S. 2008, *ApJ*, 673, L21
 Daddi, E., Elbaz, D., Walter, F., et al. 2010, *ApJ*, 714, L118
 Davis, S. W., Jiang, Y.-F., Stone, J. M., & Murray, N. 2014, arXiv:1403.1874
 Davis, S. W., Stone, J. M., & Jiang, Y.-F. 2012, *ApJS*, 199, 9
 Davis, T. A., Young, L. M., Crocker, A. F., et al. 2014, *MNRAS*, in press, arXiv:1403.4850
 Dekel, A., & Krumholz, M. R. 2013, *MNRAS*, 432, 455
 Dobbs, C. L., Krumholz, M. R., Ballesteros-Paredes, J., et al. 2014, in *Protostars and Planets VI*, eds. H. Beuther, R. S. Klessen, C. P. Dullemond, and T. Henning, in press, arXiv:1312.3223
 Fall, S. M., Krumholz, M. R., & Matzner, C. D. 2010, *ApJ*, 710, L142
 Faucher-Giguere, C.-A., Quataert, E., & Hopkins, P. F. 2013, *MNRAS*, 433, 1970
 Federrath, C., Roman-Duval, J., Klessen, R. S., Schmidt, W., & Mac Low, M.-M. 2010, *A&A*, 512, A81
 Genzel, R., Tacconi, L. J., Gracia-Carpio, J., et al. 2010, *MNRAS*, 407, 2091
 Genzel, R., Newman, S., Jones, T., et al. 2011, *ApJ*, 733, 101
 Hanasz, M., Lesch, H., Naab, T., et al. 2013, *ApJ*, 777, L38
 Harwit, M. 1962, *ApJ*, 136, 832
 Hopkins, P. F., Quataert, E., & Murray, N. 2011, *MNRAS*, 417, 950
 Hopkins, P. F., Quataert, E., & Murray, N. 2012, *MNRAS*, 421, 3488
 Hopkins, P. F., Quataert, E., & Murray, N. 2012, *MNRAS*, 421, 3522
 Jubelgas, M., Springel, V., EnBlin, T., & Pfrommer, C. 2008, *A&A*, 481, 33
 Kennicutt, R. C., Jr. 1998, *ApJ*, 498, 541
 Kim, J., & Ryu, D. 2005, *ApJ*, 630, L45
 Kim, C.-G., Ostriker, E. C., & Kim, W.-T. 2013, *ApJ*, 776, 1
 Krumholz, M. R., & Dekel, A. 2010, *MNRAS*, 406, 112
 Krumholz, M. R. 2014, *Phys. Rep.*, 539, 49
 Krumholz, M. R., Dekel, A., & McKee, C. F. 2012, *ApJ*, 745, 69
 Krumholz, M. R., & Matzner, C. D. 2009, *ApJ*, 703, 1352
 Krumholz, M. R., & McKee, C. F. 2005, *ApJ*, 630, 250
 Krumholz, M. R., & Tan, J. C. 2007, *ApJ*, 654, 304
 Krumholz, M. R., & Thompson, T. A. 2012, *ApJ*, 760, 155
 Krumholz, M. R., & Thompson, T. A. 2013, *MNRAS*, 434, 2329
 Lacki, B. C., Thompson, T. A., Quataert, E., Loeb, A., & Waxman, E. 2011, *ApJ*, 734, 107
 Leitherer, C., et al. 1999, *ApJS*, 123, 3
 Martizzi, D., Faucher-Giguère, C.-A., & Quataert, E. 2015, *MNRAS*, 450, 504
 Murray, N., Quataert, E., & Thompson, T. A. 2005, *ApJ*, 618, 569
 Murray, N., Quataert, E., & Thompson, T. A. 2010, *ApJ*, 709, 191
 Murray, N., Ménard, B., & Thompson, T. A. 2011, *ApJ*, 735, 66
 Narayanan, D., Krumholz, M., Ostriker, E. C., & Hernquist, L. 2011, *MNRAS*, 418, 664
 Narayanan, D., Krumholz, M., Ostriker, E. C., & Hernquist, L. 2012, *MNRAS*, 421, 3127
 O'dell, C. R., York, D. G., & Henize, K. G. 1967, *ApJ*, 150, 835
 Ostriker, E. C., & Shetty, R. 2011, *ApJ*, 731, 41
 Ostriker, E. C., Stone, J. M., & Gammie, C. F. 2001, *ApJ*, 546, 980
 Ptuskin, V. S., Voelk, H. J., Zirakashvili, V. N., & Breitschwerdt, D. 1997, *A&A*, 321, 434
 Scoville, N. 2003, *Journal of Korean Astronomical Society*, 36, 167
 Scoville, N. Z., Polletta, M., Ewald, S., Stolovy, S. R., Thompson, R., & Rieke, M. 2001, *AJ*, 122, 3017

- Semenov, D., Henning, T., Helling, C., Ilgner, M., & Sedlmayr, E. 2003, *A&A*, 410, 611
- Shetty, R., & Ostriker, E. C. 2012, *ApJ*, 754, 2
- Skinner, M. A., & Ostriker, E. C. 2015, *ApJ*, 809, 187
- Socrates, A., Davis, S. W., & Ramirez-Ruiz, E. 2008, *ApJ*, 687, 202
- Strickland, D. K., & Heckman, T. M. 2009, *ApJ*, 697, 2030
- Tacconi, L. J., Neri, R., Genzel, R., et al. 2013, *ApJ*, 768, 74
- Thompson, T. A., Quataert, E., & Murray, N. 2005, *ApJ*, 630, 167
- Thompson, T. A., Fabian, A. C., Quataert, E., & Murray, N. 2014, arXiv:1406.5206
- Thornton, K., Gaudlitz, M., Janka, H.-T., & Steinmetz, M. 1998, *ApJ*, 500, 95
- Vázquez-Semadeni, E., & García, N. 2001, *ApJ*, 557, 727
- Zhang, D., & Thompson, T. A. 2012, *MNRAS*, 424, 1170
- Zhang, D., Thompson, T. A., Murray, N., & Quataert, E. 2014, *ApJ*, 784, 93
- Zhang, D., Thompson, T. A., Quataert, E., & Murray, N. 2015, arXiv:1507.01951